Renewable Energy 95 (2016) 485–494

Contents lists available at ScienceDirect

Renewable Energy

journal homepage: www.elsevier.com/locate/renene

Novel high efficient offline sensorless dual-axis solar tracker for using in photovoltaic systems and solar concentrators

Hassan Fathabadi

School of Electrical and Computer Engineering, National Technical University of Athens (NTUA), Athens, Greece

ARTICLE INFO

Article history:
Received 15 March 2016
Received in revised form
18 April 2016
Accepted 20 April 2016

Keywords:
Sun path
Solar map equations
Solar tracker
Solar energy conversion systems

ABSTRACT

In this study, a novel high accurate offline sensorless dual-axis solar tracker is proposed that can be widely used in photovoltaic systems and solar concentrators. The offline estimated data extracted from solar map equations are used by the tracker to find the sun direction where the maximum value of solar energy is captured. The solar tracker has been built, and it is experimentally verified that 19.1%–30.2% more solar energy can be captured depending on the seasons by utilizing the tracker. The contribution of this work is that the proposed offline sensorless dual-axis solar tracker not only has a very simple structure with a fabrication cost much less than sensor based solar trackers but also high accurately tracks the sun direction with a very small tracking error of only 0.43° which is less than the other sensorless and sensor based dual-axis solar trackers reported in the literature excluding the sensor based dual-axis solar trackers equipped with expensive sensors mounted on high accurate mechanical carriers. Furthermore, unlike all sensor based solar trackers, since the technique is offline, the proposed tracker does not use any feedback signal, and thus, its operation is independent from external disturbances and weather conditions such as cloudy sky.

1. Introduction

Solar energy is an important renewable energy getting more popular in many countries day by day [1]. The main defect of solar energy conversion systems is their low efficiency, so that, increasing the energy efficiency of solar energy conversion systems has been the subject of many research projects, for instance, a significant attempt has been applied to provide different maximum power point tracking (MPPT) methods [2]. Some MPPT techniques reported in the literature are Lambert *W* function-based method [3], modified genetic algorithm [4], open-circuit voltage (OCV) technique [5], power management maximum power point tracking (PM- MPPT) method [6], hybrid adaptive-fuzzy technique [7], Particle swarm optimization adaptive neuro-fuzzy inference system (PSO-ANFIS) based algorithm [8], Ripple-based extremum seeking control (ESC) method [9], current-voltage deviation technique [10], and improved version of incremental conductance (IC) method [11]. When photovoltaic (PV) modules operate under mismatching operating conditions resulted from some unavoidable factors such as shadow, cloudy sky, and manufacturing tolerances, bypass diodes cause to appear more than one maximum point on *P*–*V* characteristic, so finding the global maximum power point (MPP) becomes more difficult [12,13]. This problem can be overcome using distributed MPPT (DMPPT) in which a DC-DC converter is dedicated to the MPPT of each PV module [14–16]. Two topologies can be considered to implement a grid-connected PV power generation system, so that, each PV module of the array can deliver its own maximum power. Module-dedicated DC/AC converters often called “micro-inverters topology” [17,18] and module-dedicated DC/DC converters together with central inverters generally called “micro-converters topology” are these two topologies [19–22]. In the micro-converters topology, a hybrid MPPT (HMPPT) technique regulates both the voltages of the PV modules and the DC input voltage of the central inverters [23]. A HMPPT method with the capability of high MPPT efficiency and tracking speed was presented in Ref. [24]. Non-isolated DC/DC boost converters [25] and DC/DC boost converters with isolation transformer [26] are the two main topologies widely used for DMPPT in PV systems. Different types of non-isolated DC/DC boost converters are also available that three basic types were compared from both efficiency and reliability viewpoints in Ref. [27]. A comparative study between synchronous and diode rectification boost converters showed that a synchronous rectification boost converter used for DMPPT provides

E-mail address: h4477@hotmail.com.

http://dx.doi.org/10.1016/j.renene.2016.04.063
0960-1481/

Nomenclature

d	number of days since the start of the year
D_S	duty ratio of the DC/PWM converter
LST	local solar time (hour)
f_i	switching frequency of the DC/PWM converter (Hz)
$I_L(t)$	load current of the DC/PWM converter (A)
I_{L-DC}	average (DC component) of the load current (A)
I_{pv}	PV module current (A)
L_{pv}	inductance of the inductor used in the PV filter (H)
R_{ds}	static drain to source on-resistance of MOSFET switch S (Ω)
t_{S-on}	turn-on time of MOSFET switch S (sec.)
T_i	switching period of the DC/PWM converter (sec.)
V_{pv}	PV module voltage (V)
α	altitude angle (degree)
β	azimuth angle (degree)
δ	declination angle (degree)
ϕ	latitude of the solar tracker location (degree)

more efficiency together with better thermal behavior while a diode rectification boost converter is more reliable [28]. A DMPPT method implemented by synchronous rectification boost converters was proposed in Ref. [29]. The method uses genetic algorithm to obtain the best synchronous rectification by considering a multi-objective function.

A PV module/panel/array or solar concentrator converts solar energy into electric or thermal energy [30]. To extract the maximum output power from a PV module or solar concentrator, a solar tracker can be used to track the sun direction where sunbeam is perpendicular to the face of the PV module or solar concentrator, and the maximum value of solar energy is captured [31,32]. For PV systems, previous researches showed that about 20%–50% more solar energy can be captured depending on the geographic location by adding a solar tracker to a PV system [33]. Solar trackers are divided into two types: single-axis and dual-axis [34]. The sole axis of a single-axis solar tracker is aligned along the local north meridian, it has only one freedom degree, so it can only track the sun in one direction which is the daily path of the sun [35]. A dual-axis solar tracker has two freedom degrees, so it can track the sun path in two directions which are daily and seasonal motions of the sun [36]. A single-axis solar tracking system increases the daily output power of the PV module up to about 20% compared to a fixed PV module [37]. It is clear that a dual-axis solar tracking system is more accurate to track the sun direction compared to a single-axis type [38]. A dual-axis solar tracker was implemented in Ref. [39], and it was shown that tracking flat plate PV arrays increases the captured power about 33% compared to fixed PV arrays. Single- and dual-axis trackers are classified into two types: sensor based and sensorless solar trackers. A sensor based solar tracker acts as a closed loop system in which photo sensors are used to provide appropriate feedback signals for tracking the sun direction using a feedback control system [40]. For instance, a single-axis solar tracker which uses two light-dependent resistor (LDR) sensors to provide a feedback signal to obtain the correct azimuth angle showing the daily path of the sun [41]. In high accurate sensor based dual-axis solar trackers, the sensors equipped with radiance limiting tubes are carried and oriented by a separate dual-axis mechanical system to find the sun direction, and then, the correct angles of the sun position obtained by the sensors are used by the solar tracker to orient the PV module or solar concentrator face toward the sun [42]. Thus, two independent dual-axis mechanical systems are needed; one for carrying the sensors, and the other one for PV module or solar concentrator. It is clear that the reference points of the two mechanical systems should be identical. A parallel mechanical mechanism investigated by utilizing Grassmann line geometry was proposed in Ref. [43]. The design reduces the driving torque needed for rotating the solar mirror or PV panel mounted on a dual-axis solar tracker. If high accurate equipped sensors are used, the tracking error of a sensor based dual-axis solar tracker can be limited up to 0.15° [44]. However, using cheap sensors without radiance limiting tubes or mounting them on the PV module or solar concentrator not only significantly increases the tracking error but also reduces the system robustness. For instance, a sensor based dual-axis solar tracker designed using a simple four-quadrant LDR sensor beside a cylinder all attached to the PV panel was reported in Ref. [45]. The shadow of the cylinder on the four LDRs is used to provide two feedback signals; one for azimuth angle and the other one for altitude angle. A similar dual-axis solar tracker which uses the effect of shadow on four LDRs was proposed in Ref. [46]. It is clear that the tracking error of these kinds of sensor based dual-axis solar trackers is even more than 1°. A sensorless dual-axis solar tracker acts as an open loop system, it uses the offline estimated data about the sun path in the sky obtained from different sun path charts or solar map equations [47]. For a high qualified sensorless dual-axis solar tracker, a tracking error of up to 0.45° is achievable [48], and a new set of data is also needed by changing the geographical location of the PV module or solar concentrator. The implementation of a small-sized sensorless dual-axis solar tracker which uses the azimuth and altitude angles provided by a database was reported in Ref. [49]. Although, there is no report about the tracking error, a test performed for seven hours showed that about 26% more energy can be captured by utilizing the tracker compared to a flat-positioned PV module. Based on two mathematical models; Evans and simplified type, a probabilistic model was presented to estimate the energy production of dual-axis solar trackers [50].

In this paper, a novel offline sensorless dual-axis solar tracker is proposed. The tracker can be used in photovoltaic systems and solar concentrators. It has been constructed, and experimental results are presented to evaluate its performance from different viewpoints. The proposed solar tracker is a low cost tracker with a very simple structure that high accurately performs tracking the sun direction with a very small tracking error of only 0.43° which is not only less than the other sensorless dual-axis solar trackers reported in the literature but also even less than many commercial sensor based dual-axis solar trackers. Moreover, the tracker uses offline data, so there is not any feedback signal, and thus, external disturbances and weather conditions such as cloudy sky do not have any impact on the system operation, i.e. the tracker is completely robust to external disturbances [51]. The rest of this paper is organized as follows. The design and implementation of the proposed offline sensorless solar tracker is performed in Section 2. Experimental results and cost analysis are presented in Section 3, and the paper is concluded in Section 4.

2. Implementation of the proposed offline sensorless dual-axis solar tracker

The schematic diagram of the PV system including the proposed solar tracker is shown in Fig. 1. The solar tracker consists of a controller, the stepper motor 1 which adjusts the altitude angle of the PV module/panel, the stepper motor 2 that adjusts azimuth angle, the altitude gear box that rotates the PV module/panel in the vertical plane around the altitude axis, and the azimuth gear box which similarly rotates the PV module/panel in the horizon plane

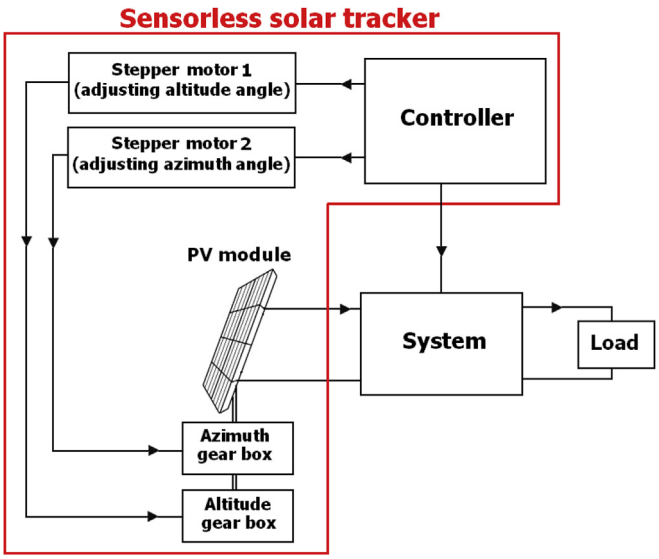

Fig. 1. Schematic diagram of the PV system including the proposed offline sensorless dual-axis solar tracker.

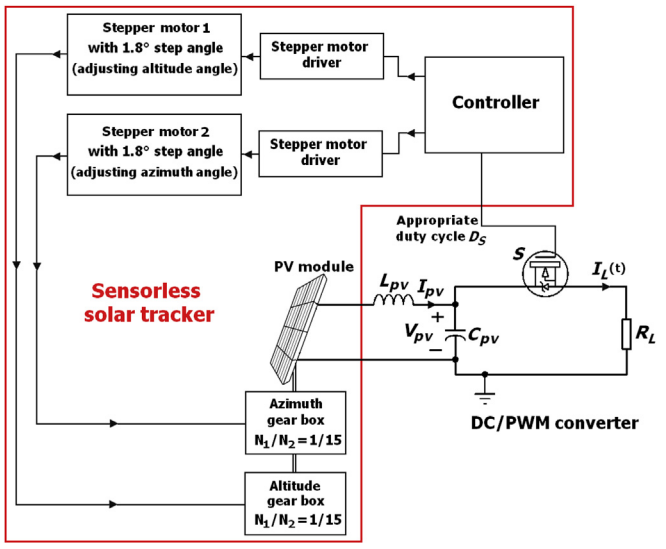

Fig. 2. Structure of the PV system constructed to implement the proposed offline sensorless dual-axis solar tracker.

around the azimuth axis. The controller continually calculates the altitude, and produces a set of appropriate control signals for the two stepper motors. The declination angle is first calculated by the controller as [52]:

$$\delta = \sin^{-1}\left(\sin(23.45^{\circ})\sin\left(\frac{360}{365}(d-81)\right)\right) \quad (1)$$

where d is number of days since the start of the year, for instance, January 1 is taken into account as $d = 1$. The altitude angle is then obtained as [53]:

$$\alpha = \sin^{-1}(\sin(\delta)\sin(\phi) + \cos(\delta)\cos(\phi)\cos(15^{\circ}(LST - 12))) \quad (2)$$

After that, the azimuth angle is found as:

$$\beta = \cos^{-1}\left(\frac{\sin(\delta)\cos(\phi) - \cos(\delta)\sin(\phi)\cos(15^{\circ}(LST-12))}{\cos(\alpha)}\right) \quad (3)$$

The structure of the PV system constructed to implement the proposed solar tracker is shown in detail in Fig. 2. It consists of a PV module, a DC/PWM converter, a controller, two stepper motor drivers, two stepper motors, and two gear boxes that each component is explained in detail as follows.

A) Stepper motors: Two identical stepper motors with the step angle of 1.8° have been used; one for adjusting altitude angle, and the other one for adjusting azimuth angle.

B) Stepper motor drivers: Two identical stepper motor drivers have been dedicated to the two stepper motors. Each driver supplies appropriate control signals and supply voltage to the associated stepper motor, so that, the stepper motor rotates according to the direction and the steps number requested by the controller.

C) DC/PWM converter: The simple DC/PWM converter used in the constructed system is shown in Fig. 2. It consists of only one MOSFET switch S that switches with a constant switching period of $T_i = {}^{1}/_{f_i}$, and a duty ratio of $D_S = t_{S-on}/T_i$. When S is turned on, the load current $I_L(t)$ flows through S and arrives to the load (R_L). When S is turned off, $I_L(t)$ immediately reaches zero, so during t_{S-on}, the load current $I_L(t)$ is expressed as:

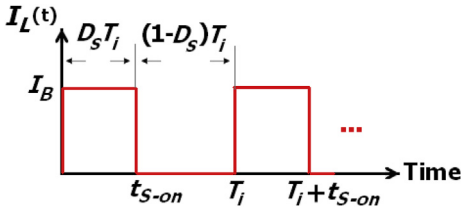

Fig. 3. Waveform of the load current $I_L(t)$.

$$I_L(t) \approx \frac{V_{pv}}{R_{ds} + R_L} = I_B \quad (4)$$

In the steady state, V_{pv} is approximately constant, and the voltage loss across L_{pv} is negligible, so $I_L(t)$ can be considered as a constant current I_B during t_{S-on}. This means that $I_L(t)$ can be estimated as the PWM waveform shown in Fig. 3. The average (DC component) of the load current can be obtained as:

$$I_{L-DC} = D_S\frac{V_{pv}}{R_{ds} + R_L} \approx D_S I_B \quad (5)$$

It is deduced from Eq. (5) that the duty ratio D_S is a control signal which adjusts the DC load current to a specific level according to the load demand.

D) Controller: The controller continually calculates the altitude and azimuth angles using Eqs. (1)–(3), and then produces the control signals which should be supplied to the two stepper motor

Table 1
Parameters of the PV circuit, and the specifications of the PV module KC200GT connected to the constructed PV system.

PV module KC200GT		DC/PWM converter	
Current at MPP I_{pv-mpp} (A)	7.61	f_i (kHz)	10
Voltage at MPP V_{pv-mpp} (V)	26.3	MOSFET switch S	IRF1407
Output power at MPP P_{pv-mpp} (W)	200.1430	**PV filter**	
Short-circuit current I_{SC} (A)	8.21	C_{pv} (μ F)	470
Open-circuit voltage V_{OC} (V)	32.9	L_{pv} (μ H)	820
Stepper motor		**Stepper motor driver**	
NEMA 23		AMIS-30543	

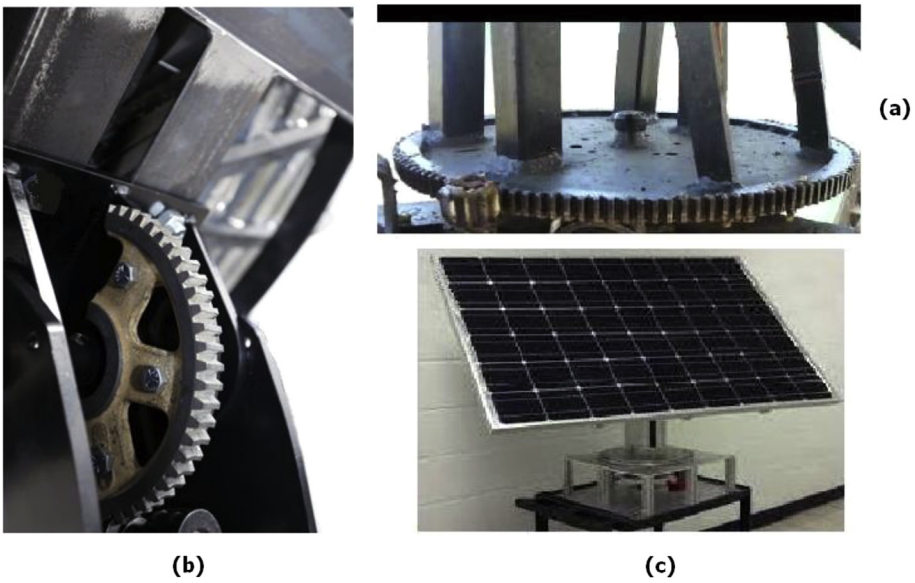

Fig. 4. Mechanical components of the constructed solar tracker: a) Azimuth gear box b) Altitude gear box c) Assembled mechanical part together with the PV module KC200GT installed on it.

drivers to rotate the two stepper motors in correct directions. Based on the calculated altitude and azimuth angles, the rotation angle of each stepper motor, and hence the associated steps number of each stepper motor is determined by the controller. The controller also produces an appropriate duty ratio D_S to be delivered to the DC/PWM converter according to the load demand.

E) PV module: One commercial PV module Kyocera KC200GT has been used in this study. The technical specifications of PV module Kyocera KC200GT under STC (standard test condition: Solar irradiance $G = 1000$ W m^{-2}, air mass (AM) 1.5 solar radiation spectrum, cell temperature $T = 25$ °C, and solar angle $\theta_z = 48.19$) extracted from its datasheet are summarized in Table 1.

F) Mechanical components: The mechanical components of the system are the two identical gear boxes shown in Fig. 2. The altitude gear box is used for rotating the PV module in the vertical plane around the altitude axis, and the azimuth gear box rotates the

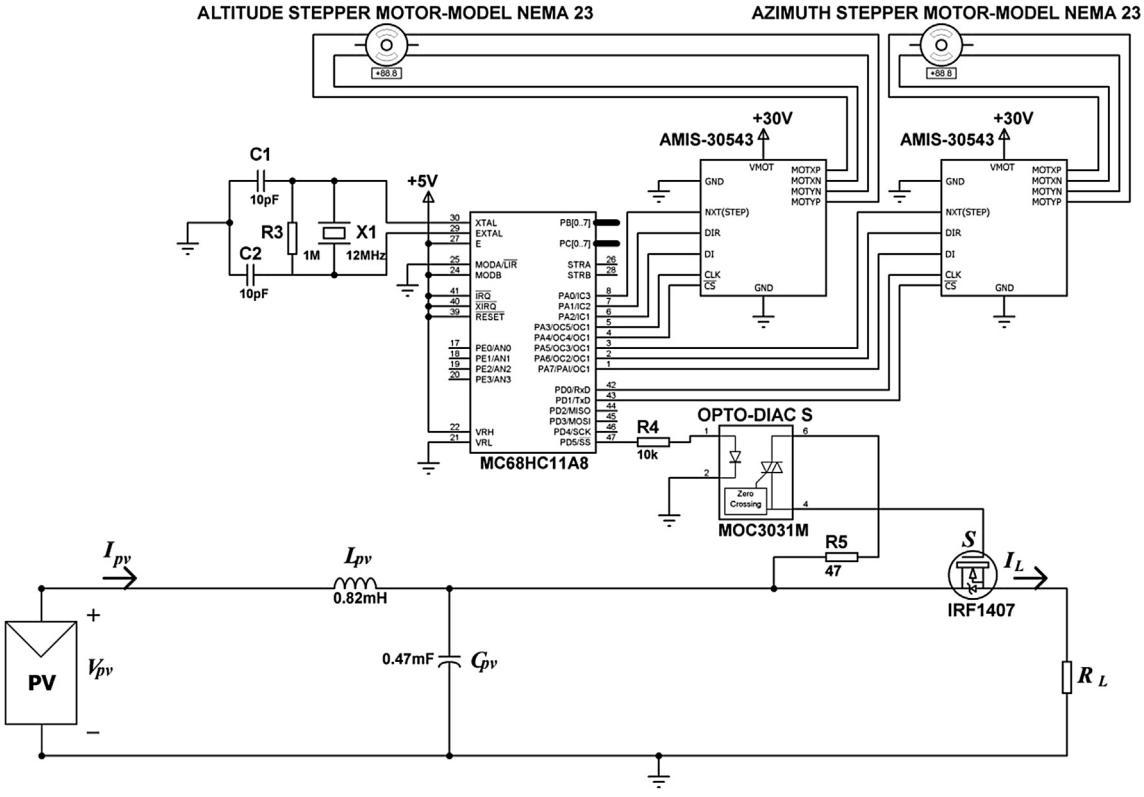

Fig. 5. Electrical circuit of the constructed PV system including the electrical part of the proposed solar tracker.

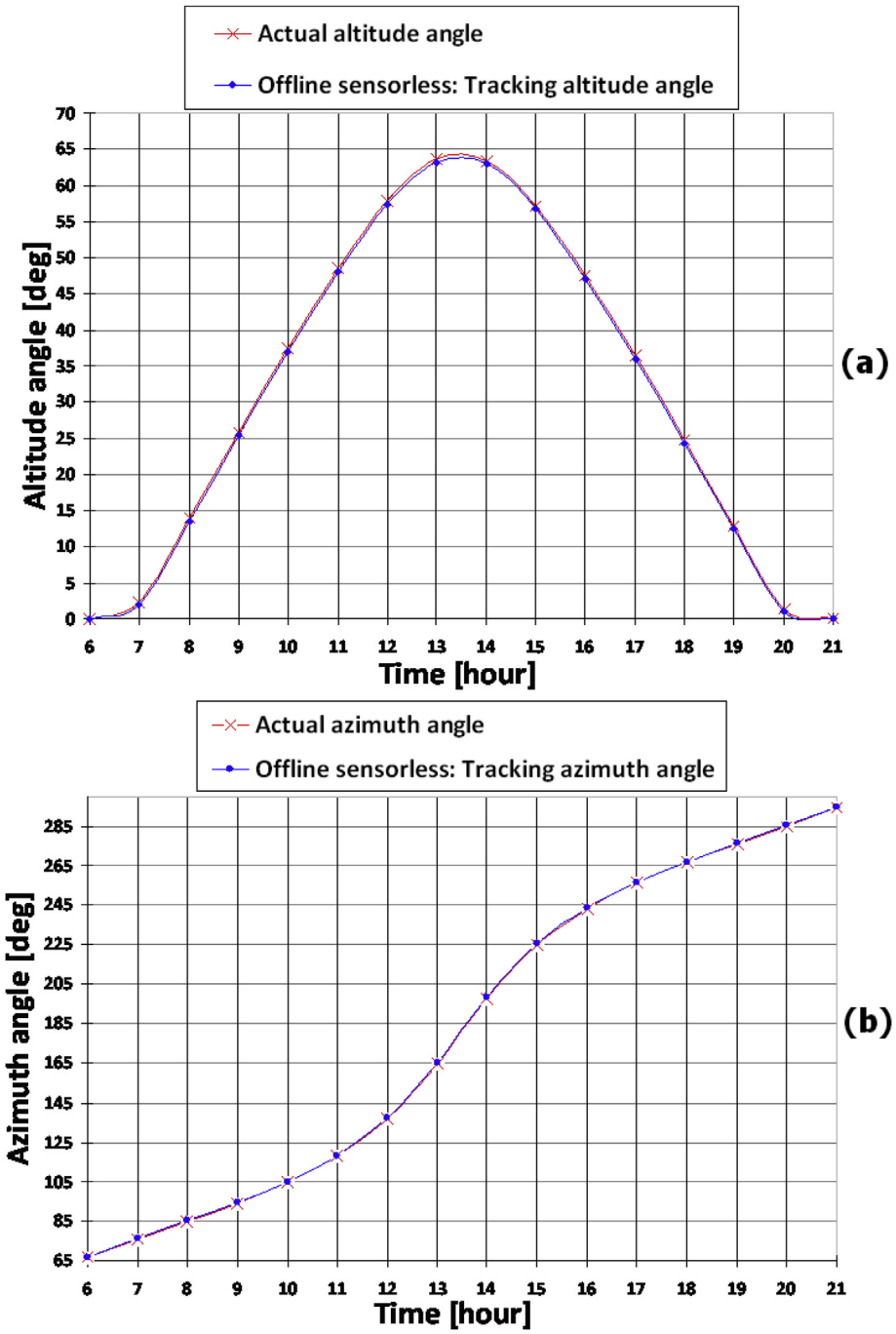

Fig. 6. Comparing between the actual altitude and azimuth angles measured from hour to hour in daylight (6:00–21:00) on Aug. 19, 2015 and the angles tracked by the proposed solar tracker.

PV module in the horizon plane around the azimuth axis. Thus, the altitude gear box has been installed horizontally on the PV module axis while the azimuth gear box has been placed vertically as shown in Fig. 4(a)-(b). Each gear box consists of two gearwheels; one primary gearwheel, and one secondary gearwheel with the gear ratio of $N_1/N_2 = 1/15$. The advantages of utilizing these two gear boxes are:

- Each stepper motor has a step angle of 1.8°, and its dedicated gearbox has a gear ratio of 1/15, so each rotation step of the stepper motor (1.8°) is converted into a rotation step of 0.12° on the secondary shaft of the gearbox coupled to the PV module/panel. This provides a very small rotation step of only 0.12° for rotating the PV module/panel around the altitude and azimuth axes, and thus, significantly decreases the tracking error.
- Since the gear ratio is $N_1/N_2 = 1/15$, each gear box increases the holding torque of the associated stepper motor by a factor of 15. Thus, the driving torque on the secondary shaft of the gearbox used to rotate the PV module/panel significantly increases. For instance, each stepper motor used in this study has the holding torque of 9 kg-cm, so the

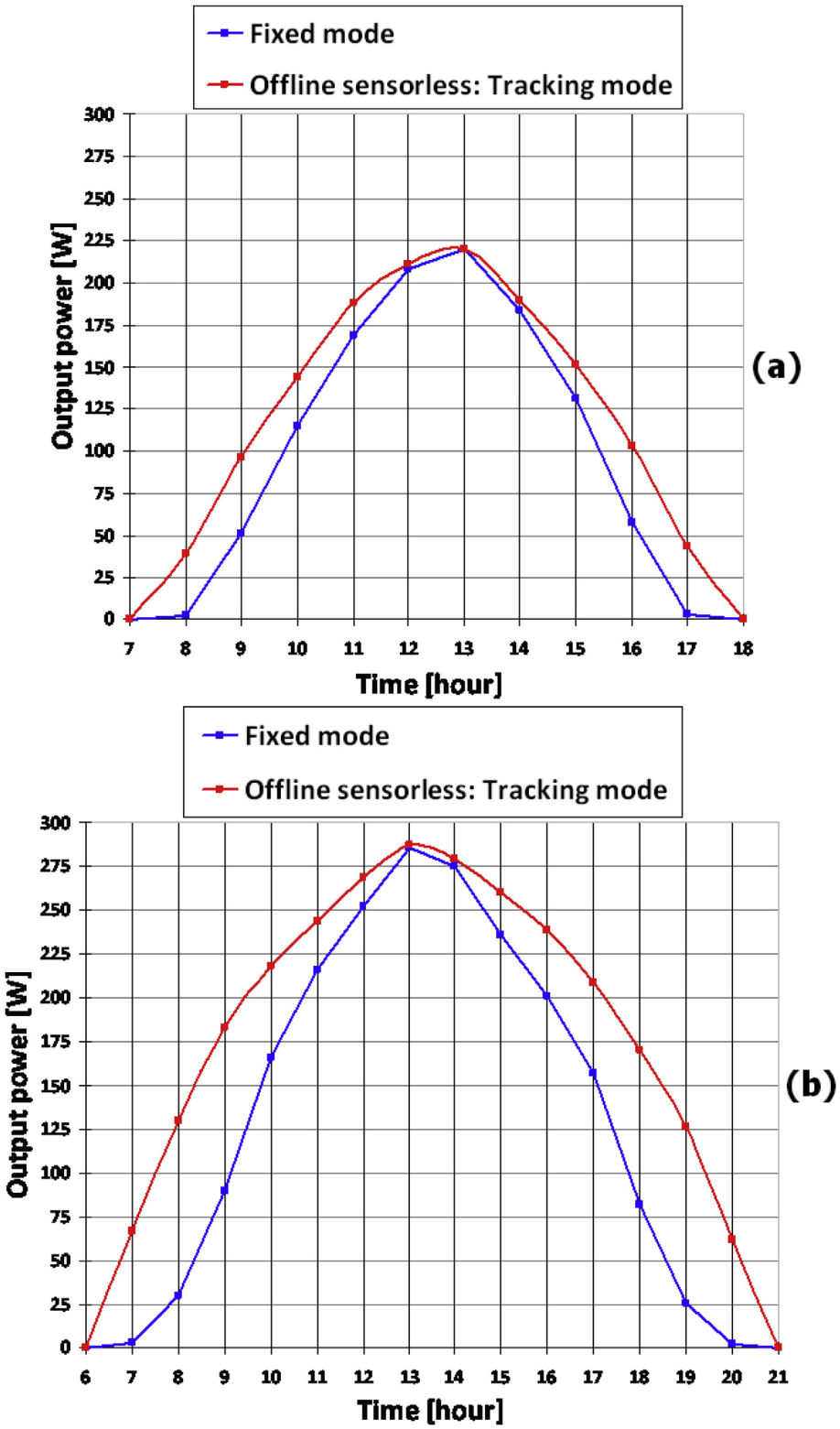

Fig. 7. Comparing between the daily output powers of the PV module on the offline sensorless tracking mode and fixed mode: a) On Jan. 19, 2014 in winter b) On Aug. 19, 2015 in summer.

driving torque is about 135 kg-cm which is great enough to move even heavy and large PV panels in practical applications.

- A combination of a gear box coupled to a stepper motor allows us not to use any brake system or torque reducer, and this not only significantly decreases the fabrication cost but also simplifies the solar tracker structure.
- Each gear box consists of only two very simple gearwheels as shown in Fig. 4(a), (b), so in practice, there is not any cost or problem for maintaining them.

Table 2
Average daily electric energy produced by the PV module in the four seasons, and increase in energy efficiency resulted from utilizing the proposed offline sensorless solar tracker.

Time	Average daily electric energy produced by the PV module [kWh]		Increase in energy efficiency (%)
	Fixed mode	Proposed offline sensorless tracking mode	
Spring	1.5764	1.9295	22.4
Summer	2.0220	2.6321	30.2
Autumn	1.7314	2.1833	26.1
Winter	1.1422	1.3599	19.1
During one year	1.6180	2.0159	24.59

The assembled mechanical part of the solar tracker together with the PV module KC200GT installed on it is shown in Fig. 4(c).

3. Experimental results: performance evaluation and cost analysis

A PV system has been built to experimentally evaluate the performance of the proposed solar tracker. The electrical circuit of the PV system constructed to implement the solar tracker is shown in Fig. 5. The controller has been implemented using a microcontroller MC68HC11A8. The opto-diac S delivers a periodic switching pulse with the period of $T_i = 100$ μs ($f_i = 10$ kHz) and the duty ratio of D_S produced and regulated by the microcontroller according to the load demand. The microcontroller MC68HC11A8 calculates the altitude and azimuth angles using Eqs. (1)–(3), and then produces the ten control signals to be delivered to the two stepper motor drivers to rotate the two stepper motors in correct directions with appropriate rotation angles. Based on the calculated altitude and azimuth angles, the rotation angle, and hence the associated steps number of each stepper motor is determined by the microcontroller to track the sun direction in the sky. Two stepper motor drivers AMIS-30543 have been used; one for driving the altitude stepper motor, and the other one for driving the azimuth stepper motor. Each deriver has been connected to the microcontroller through the five wires, and receives five control signals from the controller. Two stepper motors NEMA 23 with the holding torque of 9 kg-cm have been also used; one for adjusting the altitude angle α, and the other one for azimuth angle β. In each step of the tracking process, the microcontroller MC68HC11A8 produces and supplies five control signals to each driver. These control signals cause a rotation step of 1.8° on the shaft of each stepper motor in the correct direction that is converted into a rotation step of 0.12° by the dedicated gear box, and rotates the PV module/panel around the altitude/azimuth axis. The above process is repeated until the altitude and azimuth angles both to be equal to the calculated angles. The technical specifications of the different parts of the constructed PV system are also summarized in Table 1.

3.1. Performance evaluation

The constructed solar tracking system was activated. The actual altitude and azimuth angles of the sun position in the sky observed from the PV module situated in the geographic location of (37.9667° N, 23.7167° E) were measured from hour to hour in daylight (6:00–21:00) on Aug. 19, 2015 using two digital protractors; one for measuring the altitude angle and the other one for the azimuth angle. Fig. 6(a)-(b) compare the actual altitude and azimuth angles of the sun direction to the altitude and azimuth angles tracked by the proposed offline sensorless dual-axis solar tracker. The comparison shows that the maximum absolute value of the tracking error is 0.43°, so the tracking error of the tracker is 0.43° in tracking the azimuth and altitude angles.

In other experiment, the daily output power of the PV module was measured from hour to hour in daylight on Jan. 19, 2014 in winter (temperature = 18°, humidity = 59%, wind speed = 1 km/h) and on Aug. 19, 2015 in summer (temperature = 31°, humidity = 27%, wind speed = 14 km/h). Each measurement was performed twice; at the first time, it was measured when the solar tracker was active (offline sensorless tracking mode). At the second time, it was measured when the solar tracker was off, and the PV module was fixed at the noon position of the sun (fixed mode). The daily output powers measured in winter and summer for both the offline sensorless tracking and fixed modes are shown in Fig. 7 (a) and Fig. 7(b), respectively. It can be seen from Fig. 7(a) that in winter, the daily electric energies produced by the PV module on the fixed and offline sensorless tracking modes are respectively about 1.1422 kWh and 1.3599 kWh, and thus, the solar energy converted on the offline sensorless tracking mode is 19.1% more than that on the fixed mode. Similarly, Fig. 7(b) shows that the daily electric energies obtained on the fixed and offline sensorless tracking modes are respectively about 2.0220 kWh and 2.6321 kWh in summer, so there is an increase of 30.2% in the energy efficiency on the offline sensorless tracking mode. The above-mentioned daily energy measurements and the other measurements related to spring and autumn are summarized in Table 2. On the one hand, in the morning and afternoon, the PV module fixed at the noon position receives sunlight in incorrect direction. On the other hand, not only daytime in summer (15 h) is more than that in other seasons, for instance, only 11 h in winter but also solar irradiance in summer is more than that in other seasons, so the increase in the solar energy captured in summer is more than that in other seasons as verified by the real experimental data reported in Table 2. In addition to the power, the PV module currents were also measured from hour to hour on the offline sensorless tracking and fixed modes which are shown in Fig. 8. The variation of the PV module current versus the azimuth angle on the two modes is also shown in Fig. 9.

Table 3 compares the solar tracker proposed in this study is compared with the several typical dual-axis solar trackers reported in the literature. The comparison shows that the proposed tracker has not only a fabrication cost less than the sensor based solar trackers but also a very small tracking error of only 0.43° which is less than the other sensorless and sensor based dual-axis solar trackers.

3.2. Cost analysis and economic benefits

As shown in Fig. 2, the proposed offline sensorless dual-axis solar tracker is implemented by adding only two stepper motors, two stepper motor drivers, and two gear boxes to the conventional system. In the constructed system shown in Fig. 5, the prices of the added components are $80 (two stepper motors NEMA 23), $40 (two stepper motor drivers AMIS-30543), and $70 (two gear boxes), and so the total price is only about $190. On the one hand, this fabrication cost is much less than a high accurate sensor based dual-axis solar tracker because the sensor based version needs

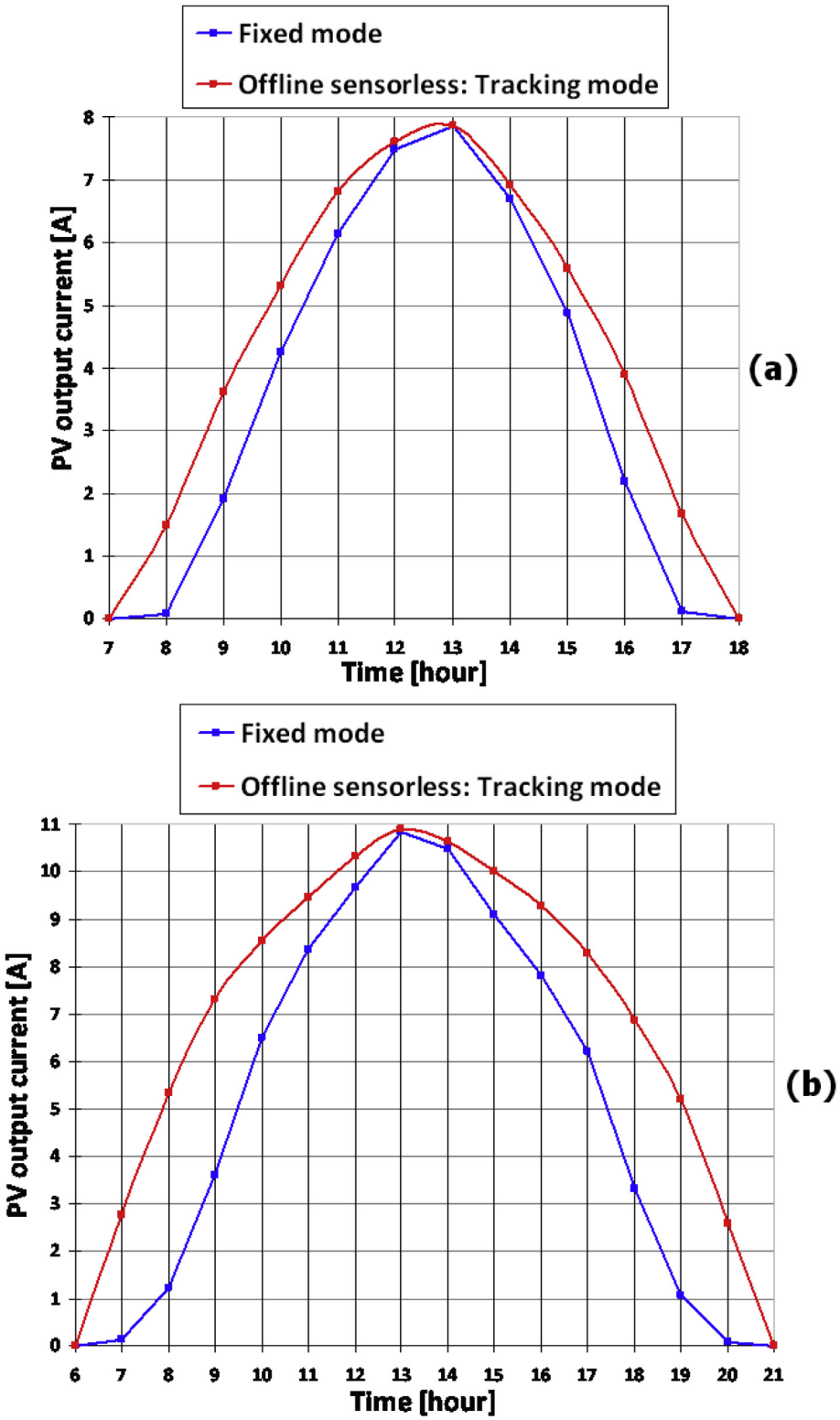

Fig. 8. PV module current on the offline sensorless tracking mode and fixed mode: a) On Jan. 19, 2014 in winter b) On Aug. 19, 2015 in summer.

some additional units consisting of an irradiance sensor equipped with a radiance limiting tube, and an independent dual-axis mechanical system for carrying the sensor and its radiance limiting tube. On the other hand, Table 2 shows that the only PV module KC200GT used in the constructed system produces the average daily electric energies of 1.6180 kWh and 2.0159 kWh respectively on the fixed and tracking modes during one year. Thus, the extra daily electric energy obtained by utilizing the proposed solar tracker is 0.4 kWh. Since the average electricity price around the world is 0.2 $/kWh, the price of the extra daily electric energy is $0.08. Comparing this price with the solar tracker price ($190) shows that utilizing the tracker with even one PV module returns

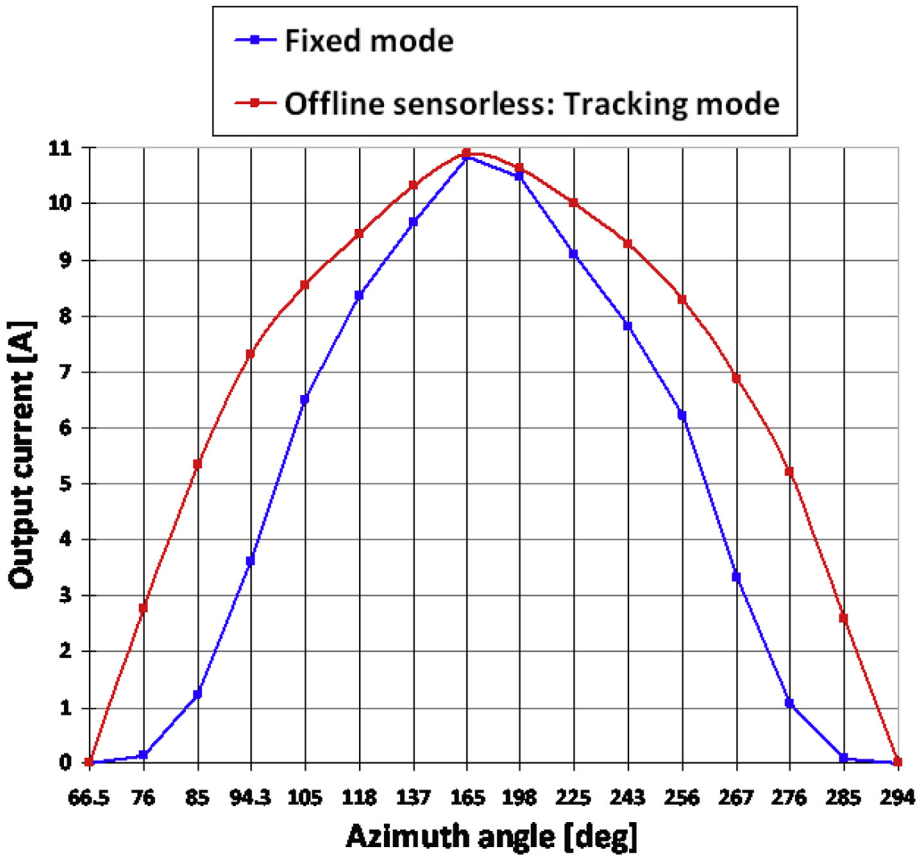

Fig. 9. PV module current versus the azimuth angle for the offline sensorless tracking and fixed modes on Aug. 19, 2015 in summer.

Table 3
Comparison between the proposed solar tracker and several typical solar trackers.

Dual-axis solar tracker type	Sensor based [42]	Sensor based [45]	Sensor based [46]	Sensorless [47]	Sensorless [48]	Sensorless [this work]
Tracking error	2°	>1°	>1°	Not reported	Not reported	0.43°
Fabrication cost with reference to this work	More	More	More	Same	Same	–

its cost ($190) after only 2375 days ($190 ÷$0.08 = 2375 days). In practical applications, the tracker is used with a large PV panel, so its cost comes back much sooner. For instance, installing the proposed solar tracker on a PV panel consisting of 16 PV modules returns the tracker cost after only 149 days, and this explicitly verifies its economic benefit.

4. Conclusion

In this paper, a novel high accurate offline sensorless dual-axis solar tracker was presented. It was experimentally verified that 24.59% more solar energy is captured during one year by utilizing the solar tracker. Very simple structure, very low fabrication cost which is much less than sensor based solar trackers, and very small tracking error of only 0.43° which is less than the other sensorless and sensor based dual-axis solar trackers reported in the literature except the high accurate sensor based dual-axis solar trackers equipped with expensive equipments are the three excellent specifications of the proposed solar tracker. Moreover, the tracker is completely robust to external disturbances. As future work, since the mechanical part of the tracker operates high accurately, it can be used to design and implement very high accurate sensor based trackers.

References

[1] E. Díaz-Dorado, A. Suárez-García, C.J. Carrillo, J. Cidrás, Optimal distribution for photovoltaic solar trackers to minimize power losses caused by shadows, Renew. Energy 36 (6) (2011) 1826–1835.
[2] H. Rezk, A.M. Eltamaly, A comprehensive comparison of different MPPT techniques for photovoltaic systems, Sol. Energy 112 (2015) 1–11.
[3] H. Fathabadi, Lambert *W* function-based technique for tracking the maximum power point of PV modules connected in various configurations, Renew. Energy 74 (2015) 214–226.
[4] S. Daraban, D. Petreus, C. Morel, A novel MPPT (maximum power point tracking) algorithm based on a modified genetic algorithm specialized on tracking the global maximum power point in photovoltaic systems affected by partial shading, Energy 74 (2014) 374–388.
[5] J.H.R. Enslin, M.S. Wolf, D.B. Snyman, W. Swiegers, Integrated photovoltaic maximum power point tracking converter, IEEE Trans. Ind. Electron. 44 (1997) 769–773.
[6] M. Orabi, F. Hilmy, A. Shawky, J.A.A. Qahouq, E.-S. Hasaneen, E. Gomaa, On-chip integrated power management MPPT controller utilizing cell-level architecture for PV solar system, Sol. Energy 117 (2015) 10–28.
[7] O. Guenounou, B. Dahhou, F. Chabour, Adaptive fuzzy controller based MPPT for photovoltaic systems, Energy Convers. Manag. 78 (2014) 843–850.
[8] M. Muthuramalingam, P.S. Manoharan, Comparative analysis of distributed MPPT controllers for partially shaded stand alone photovoltaic systems, Energy Convers. Manag. 86 (2014) 286–299.
[9] I. Munteanu, A.I. Bratcu, MPPT for grid-connected photovoltaic systems using ripple-based Extremum Seeking Control: analysis and control design issues, Sol. Energy 111 (2015) 30–42.
[10] H. Fathabadi, Novel fast dynamic MPPT (maximum power point tracking) technique with the capability of very high accurate power tracking, Energy 94

(2016) 466–475.
[11] K.S. Tey, S. Mekhilef, Modified incremental conductance MPPT algorithm to mitigate inaccurate responses under fast-changing solar irradiation level, Sol. Energy 101 (2014) 333–342.
[12] C. Olalla, C. Deline, D. Maksimovic, Performance of mismatched PV systems with submodule integrated converters, IEEE J. Photovolt. 4 (1) (2014) 396–404.
[13] S.M. MacAlpine, R.W. Erickson, M.J. Brandemuehl, Characterization of power optimizer potential to increase energy capture in photovoltaic systems operating under nonuniform conditions, IEEE Trans. Power Electron. 28 (6) (2013) 2936–2945.
[14] R.C.N. Pilawa-Podgurski, D.J. Perreault, Submodule integrated distributed maximum power point tracking for solar photovoltaic applications, IEEE Trans. Power Electron. 28 (6) (2013) 2957–2967.
[15] N. Femia, G. Lisi, G. Petrone, G. Spagnuolo, M. Vitelli, Distributed maximum power point tracking of photovoltaic arrays: novel approach and system analysis, IEEE Trans. Ind. Electron. 55 (7) (2008) 2610–2621.
[16] M. Vitelli, On the necessity of joint adoption of both distributed maximum power point tracking and central maximum power point tracking in PV systems, Prog. Photovolt. Res. Appl. 22 (3) (2014) 283–299.
[17] S.B. Kjaer, J.K. Pedersen, F. Blaabjerg, A review of single-phase grid-connected inverters for photovoltaic modules, IEEE Trans. Ind. Appl. 41 (5) (2005) 1292–1306.
[18] Q. Li, P. Wolfs, A review of the single phase photovoltaic module integrated converter topologies with three different DC link configurations, IEEE Trans. Power Electron. 23 (3) (2008) 1320–1333.
[19] J. Huusari, T. Suntio, Origin of cross-coupling effects in distributed DC-DC converters in photovoltaic applications, IEEE Trans. Power Electron. 28 (10) (2013) 4625–4635.
[20] S. Vighetti, J.-P. Ferrieux, Y. Lembeye, Optimization and design of a cascaded DC/DC converter devoted to grid-connected photovoltaic systems, IEEE Trans. Power Electron. 27 (4) (2012) 2018–2027.
[21] S. Poshtkouhi, V. Palaniappan, M. Fard, O. Trescases, A general approach for quantifying the benefit of distributed power electronics for fine grained MPPT in photovoltaic applications using 3D modeling, IEEE Trans. Power Electron. 99 (11) (2011) 4656–4666.
[22] C. Olalla, M. Rodriguez, D. Clement, D. Maksimovic, Architectures and control of submodule integrated DC-DC converters for photovoltaic applications, IEEE Trans. Power Electron. 28 (6) (2013) 2980–2997.
[23] T. Esram, P.L. Chapman, Comparison of photovoltaic array maximum Power Point Tracking techniques, IEEE Trans. Energy Convers. 22 (2) (2007) 439–449.
[24] G. Aurilio, M. Balato, G. Graditi, C. Landi, M. Luiso, M. Vitelli, Fast hybrid MPPT technique for photovoltaic applications: numerical and experimental validation, Adv. Power Electron. 2014 (2014) 15. Article ID 125918.
[25] W. Li, Y. Deng, J. Liu, X. He, A review of non-isolated high step-up DC/DC converters in renewable energy applications, in: 24th Annual Applied Power Electronics Conference and Exposition (APEC) IEEE, 2009, pp. 1825–1832.
[26] Q. Li, P. Wolfs, A review of the single phase photovoltaic module integrated converter topologies with three different DC link configurations, IEEE Trans. Power Electron. (2008) 1320–1333.
[27] G. Graditi, D. Colonnese, N. Femia, Efficiency and reliability comparison of DC-DC converters for single phase grid connected photovoltaic inverters, in: SPEEDAM 2010-International Symposium on Power Electronics, Electrical Drives, Automation and Motion, 2010, pp. 140–147.
[28] G. Graditi, G. Adinolfi, N. Femia, M. Vitelli, Comparative analysis of synchronous rectification boost and diode rectification boost converter for DMPPT applications, in: ISIE 2011-IEEE International Symposium on Industrial Electronics, 2011, pp. 1000–1005.
[29] G. Adinolfi, G. Graditi, P. Siano, A. Piccolo, Multiobjective optimal design of photovoltaic synchronous boost converters assessing efficiency, reliability, and cost savings, IEEE Trans. Ind. Inf. 11 (5) (2015) 1038–1048.
[30] S. Ozdemir, N. Altin, I. Sefa, Single stage three level grid interactive MPPT inverter for PV systems, Energy Convers. Manag. 80 (2014) 561–572.
[31] S.A.S. Eldin, M.S. Abd-Elhady, H.A. Kandil, Feasibility of solar tracking systems for PV panels in hot and cold regions, Renew. Energy 85 (2015) 228–233.
[32] F. Nenciu, D.-I. Vaireanu, A comparative study for assessing the effectiveness of solar trackers used in conjunction with photovoltaic power autonomous systems, J. Optoelectron. Adv. Mater. 16 (1–2) (2014) 102–109.
[33] G. Quesada, L. Guillon, D.R. Rousse, M. Mehrtash, Y. Dutil, P.L. Paradis, Tracking strategy for photovoltaic solar systems in high latitudes, Energy Convers. Manag. 103 (2015) 147–156.
[34] F. Sallaberry, R. Pujol-Nadal, M. Larcher, M.H. Rittmann-Frank, Direct tracking error characterization on a single-axis solar tracker, Energy Convers. Manag. 105 (2015) 1281–1290.
[35] K.K. Chong, C.W. Wong, General formula for on-axis sun-tracking system and its application in improving tracking accuracy of solar collector, Sol. Energy 83 (3) (2009) 298–305.
[36] L. Barker, M. Neber, H. Lee, Design of a low-profile two-axis solar tracker, Sol. Energy 97 (2013) 569–576.
[37] A. Al-Mohammad, Efficiency improvement of photovoltaic panels using a sun tracking system, Appl. Energy 79 (3) (2004) 345–354.
[38] R. Eke, A. Senturk, Performance comparison of a double-axis sun tracking versus fixed PV system, Sol. Energy 86 (9) (2012) 2665–2672.
[39] P. Roth, A. Georgiev, H. Boudinov, Cheap two axis sun following device, Energy Convers. Manag. 46 (7–8) (2005) 1179–1192.
[40] P. Zhang, G. Zhou, Z. Zhu, W. Li, Z. Cai, Numerical study on the properties of an active sun tracker for solar streetlight, Mechatronics 23 (8) (2013) 1215–1222.
[41] C.S. Chin, A. Babu, W. McBride, Design, modeling and testing of a standalone single axis active solar tracker using MATLAB/Simulink, Renew. Energy 36 (11) (2011) 3075–3090.
[42] J. Cañadaa, M.P. Utrillasb, J.A. Martinez-Lozanob, R. Pedrósb, J.L. Gómez-Amob, A. Maja, Design of a sun tracker for the automatic measurement of spectral irradiance and construction of an irradiance database in the 330–1100 nm range, Renew. Energy 32 (12) (2007) 2053–2068.
[43] J. Wu, X. Chen, L. Wang, Design and dynamics of a novel solar tracker with parallel mechanism, IEEE/ASME Trans. Mechatron. 21 (1) (2016) 88–97.
[44] Y. Yao, Y. Hu, S. Gao, G. Yang, J. Du, A multipurpose dual-axis solar tracker with two tracking strategies, Renew. Energy 72 (2014) 88–98.
[45] J.M. Wang, C.L. Lu, Design and implementation of a sun tracker with a dual-axis single motor for an optical sensor-based photovoltaic system, Sensors 13 (3) (2013) 3157–3168.
[46] N. Barsoum, Fabrication of dual-axis solar tracking controller project, Intell. Control Autom. 2 (2011) 57–68.
[47] F. Duarte, P.D. Gaspar, L.C. Goncalves, Two axes solar tracker based on solar maps controlled by a low-power microcontroller, J. Energy Power Eng. 5 (7) (2011) 671–676.
[48] C.A. Tirmikci, C. Yavuz, Comparison of solar trackers and application of a sensor less dual axis solar tracker, J. Energy Power Eng. 9 (2015) 556–561.
[49] R. Syafii, Nazir, Kamshory, M. Hadi, Improve dual axis solar tracker algorithm based on sunrise and sunset position, J. Electr. Syst. 11 (4) (2015) 397–406.
[50] G.M. Tina, S. Gagliano, G. Graditi, A. Merola, Experimental validation of a probabilistic model for estimating the double axis PV tracking energy production, Appl. Energy 97 (2012) 990–998.
[51] C.S. Chin, Model-based simulation of an intelligent microprocessor-based standalone solar tracking system, in: Ebook: MATLAB – a Fundamental Tool for Scientific Computing and Engineering Applications, vol. 3, InTech, 2012, pp. 251–278.
[52] J.A. Duffie, W.A. Beckman, Solar Engineering of Thermal Processes, fourth ed., Wiley, 2013. ISBN: 978-0-470-87366-3.
[53] I. Reda, A. Andreas, Solar position algorithm for solar radiation applications, Sol. Energy 76 (5) (2004) 577–589.